Magnetic Property – Structure Relationships at the Nano-scale for Melt-spun and Aged SmCo-based Alloys

X.Y. Xiong[a,b] and T.R. Finlayson[c]

[a] *Monash Centre for Electron Microscopy, Monash University, Victoria 3800, Australia.*
[b] *Department of Materials Engineering, Monash University, Victoria 3800, Australia.*
[c] *School of Physics, University of Melbourne, Victoria 3010, Australia.*

The phase transformations, microstructure and magnetic properties of melt-spun $Sm(Co_{0.68}Fe_{0.2}Cu_{0.1}Zr_{0.02})_{7.5}$ alloy, following various heat treatments are reported. The microstructure was determined on various scales using XRD, TEM and 3DAP analysis while the magnetic properties have been measured using SQUID magnetometry. The optimum magnetic properties are found for an intimate cell structure comprising the $SmCo_5$ and Sm_2Co_{17}-type phases. Local compositions of the individual phases and at the phase interfaces are presented, and the effects of the changes in the microstructure on magnetic properties are discussed.

1. Introduction

SmCo-based magnets have been studied extensively on account of their superior properties for high temperature applications [1-3], with operating temperatures in excess of 500°C having been reported [2]. The microstructure of conventional, sintered, Sm_2Co_{17}-type permanent magnets containing transition metal additions comprises three phases: the rhombohedral Sm_2Co_{17} cell phase, the hexagonal $SmCo_5$ cell boundary phase, and the platelet Z-phase with rhombohedral $SmCo_3$ structure [1,4].

The high coercivity of the sintered magnets is associated with the high Cu content at the $Sm_2Co_{17}/SmCo_5$ interfaces [2]. However, the detailed mechanism for the coercivity is still open for discussion. It was found that a similar microstructure could be formed in melt-spun alloy ribbons after appropriate heat treatment [3]. As the cooling rate for the melt-spinning is much faster than the quenching rate used for the sintered alloys, the driving force for the diffusion of each of the elemental atoms in these alloys during ageing is expected to be different from that in the sintered alloys, hence the redistribution of compositions will be different.

In the present work, we studied the phase transformations, microstructure and magnetic properties of melt-spun $Sm(Co_{0.68}Fe_{0.2}Cu_{0.1}Zr_{0.02})_{7.5}$ alloy, following various heat treatments, using X-ray diffraction (XRD), transmission electron microscopy (TEM), 3D atom probe (3DAP) analysis and SQUID magnetometry.

2. Experimental techniques

Melt-spun ribbon of nominal composition $Sm(Co_{0.68}Fe_{0.2}Cu_{0.1}Zr_{0.02})_{7.5}$ was prepared using a single-roller technique in a controlled inert-gas atmosphere. Chemical analysis of the ribbon samples confirmed that the above nominal composition was achieved. Ribbon samples were heat treated in sealed, evacuated, quartz tubes at temperatures of 720, 760, 800, 840 and 900°C for 3 h, then slowly cooled to 460°C at 0.5°C/min, and water quenched. Microstructures were examined by XRD, TEM (Philips CM20) and 3DAP (Oxford NanoScience [5]). Specimens for 3DAP analysis were prepared by grinding ribbons into square rods (20 μm × 20 μm × 8 mm) and electropolishing to a sharp tip in a solution of 2% $HClO_4$ + 98% 2-butoxyethanol at a voltage of ~10 Volts.

Magnetization versus field measurements were made using a superconducting quantum interference device (SQUID) magnetometer (MPMS-7) at room temperature. The maximum applied magnetic field was 50 kOe. Samples for the magnetic measurements were rectangular sections, ~6 mm long, 1 mm wide and 30 μm thick, so that demagnetization could be neglected. Saturation magnetization, σ_s, magnetic coercivity, H_c, remanence to saturation magnetization ratio, M_r/M_s, (M_s being the magnetization at 50 kOe) and maximum energy product, $(BH)_{max}$, were determined from the magnetization versus field data.

3. Results

3.1 Magnetic Data

The changes in magnetic properties of the melt-spun ribbons before and after ageing treatment are shown in Fig. 1. H_c of the as-spun ribbon was very low, ~510 Oe, shown as the point at the ageing temperature, T_a = 20°C. After ageing at 720°C, the H_c increased to 4340 Oe, remained almost unchanged until T_a = 800°C, and then decreased at 840°C. In contrast, σ_s decreased from 84 ± 4 emu/g (for the as-spun state) to 78 ± 4 emu/g (at T_a = 760°C) but increased steadily following ageing at the higher temperatures. For $(BH)_{max}$ the overall change with the ageing temperature is similar to that of the coercivity. The highest $(BH)_{max}$ was 6.5 MGOe at T_a = 800°C. M_r/M_s was 0.49 for the as-spun ribbons, typical for isotropic alloys, and following ageing showed a broad peak having maximum value of 0.70 at T_a = 760°C.

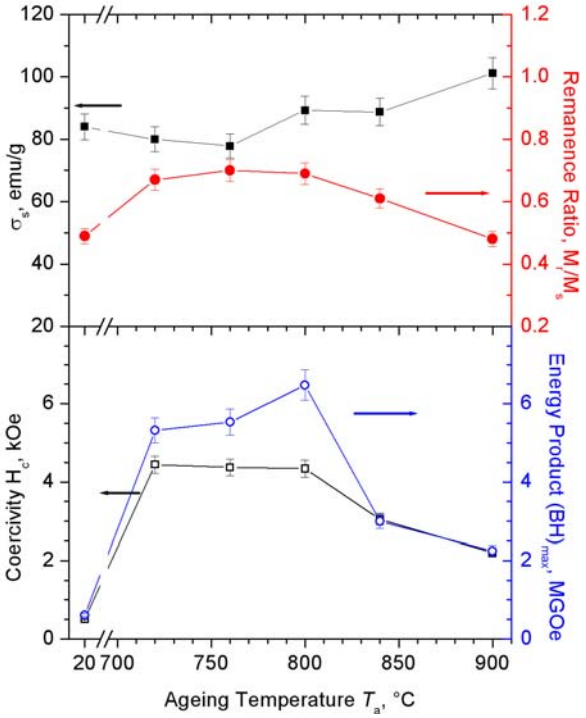

Fig. 1. Saturation magnetization, σ_s, remanence to saturation magnetization ratio, M_r/M_s, coercivity, H_c, and maximum energy product, $(BH)_{max}$, as functions of ageing temperature.

3.2 Microstructures

XRD analysis and TEM (Fig. 2) (together with selected area diffraction (SAD) patterns) showed the as-spun ribbon to be a single phase with the Cu_7Tb structure and a grain size of ~600 nm (Fig. 2(a)).

Following ageing at 720°C (Fig. 2(b)), a cellular structure comprising Sm_2Co_{17} (2:17R) and $SmCo_5$ (1:5H) type phases developed, with grain size similar to that for as-spun ribbon. The 3D atom maps of Sm and Cu following this ageing treatment (Fig. 3(a)) clearly shows two phases and by cutting a small box of dimensions

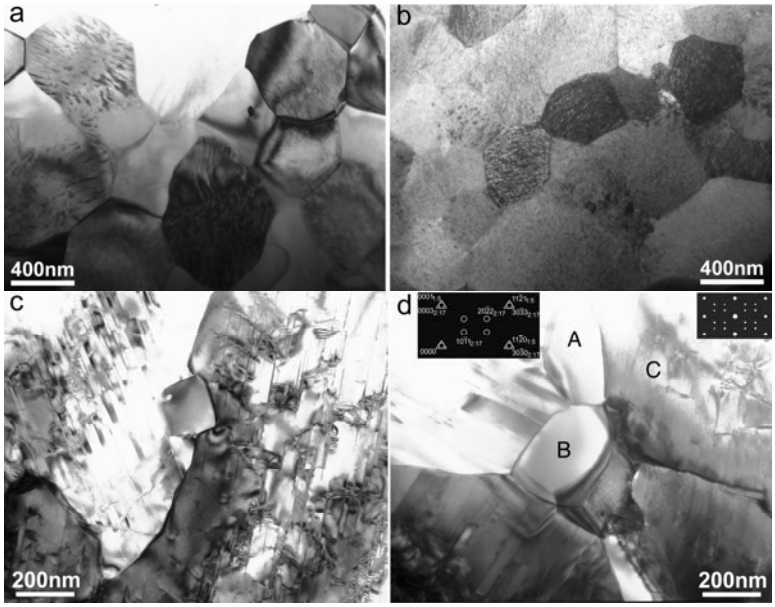

Fig. 2. TEM micrographs of samples (a) as-spun, and aged at (b) 720°C, (c) 840°C and (d) 900°C. In (d), the right inset is SAD of region C and the left a simulated pattern using the 2:17R and 1:5H structures.

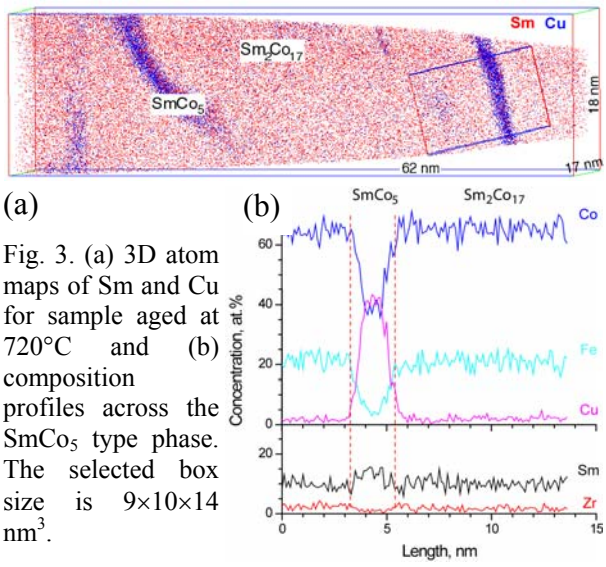

Fig. 3. (a) 3D atom maps of Sm and Cu for sample aged at 720°C and (b) composition profiles across the $SmCo_5$ type phase. The selected box size is 9×10×14 nm^3.

stacking sequence of the (0003) planes of the Sm_2Co_{17} phase, with interplanar spacing of ~0.4 nm, was observed. The Sm-rich and Co-rich layers appear alternately in the [0001] direction (Fig. 4(a) and (c)). Fig. 4(b) and (c) show the composition profiles across the $Sm_2Co_{17}/SmCo_5$ and Sm_2Co_{17}/Z-phase interfaces, respectively. The composition results for each of the respective phases as calculated from the 3DAP analysis, are listed in Table 1.

Following ageing at 900°C the 2:17R + 1:5H grains increase in size (Fig. 2(d) (grain C)) while small particles (A and B) comprising a CoFeZr-rich phase, precipitate at grain boundaries.

4. Discussion

The low coercivity for the as-spun ribbon arises from the single-phase, $Cu_{17}Tb$-type structure. Enhancement of H_c, M_r/M_s and $(BH)_{max}$ with ageing is a consequence of the transformation to the cellular structure consisting of the $SmCo_5$ and Sm_2Co_{17} type phases, but without Z-phase.

By comparing the results following 720 and 840°C ageing, it can be seen that the compositions of the $SmCo_5$ and Sm_2Co_{17} phases in the 720°C sample are similar to those in the 840°C sample. The ageing temperature did not change the phase compositions significantly, except for the Zr content, which was decreased almost by half on increasing the ageing temperature. The depletion of Zr in the two phases is understandable, as Zr was used in the formation of the Z-phase. The phase evolution sequence observed in this isochronal treatment shows that the as-spun, single-phase, Cu_7Tb structure was first transformed into two phases, Sm_2Co_{17} and $SmCo_5$. The platelet Z-phase requires a higher temperature, suggesting a

$9\times10\times14$ nm^3 across the $SmCo_5$ phase, the composition distributions in each of these phases have been analyzed (Fig. 3(b) and Table 1). In particular, the Zr concentration in the 2:17R phase was 1.9 ± 0.4 at.%, which is almost the same at that for the as-spun ribbon, 2.1 ± 0.1 at.% [6]. This result indicates that at this ageing temperature the Zr atoms remained in the matrix phase consistent with the fact that no Z-phase was observed.

The platelet Z-phase first appeared following ageing at 840°C (Fig. 2(c)) along with an increased grain size. 3DAP analysis also confirmed the Z-phase (Fig. 4(a)) and atomic-layer resolution, corresponding to the

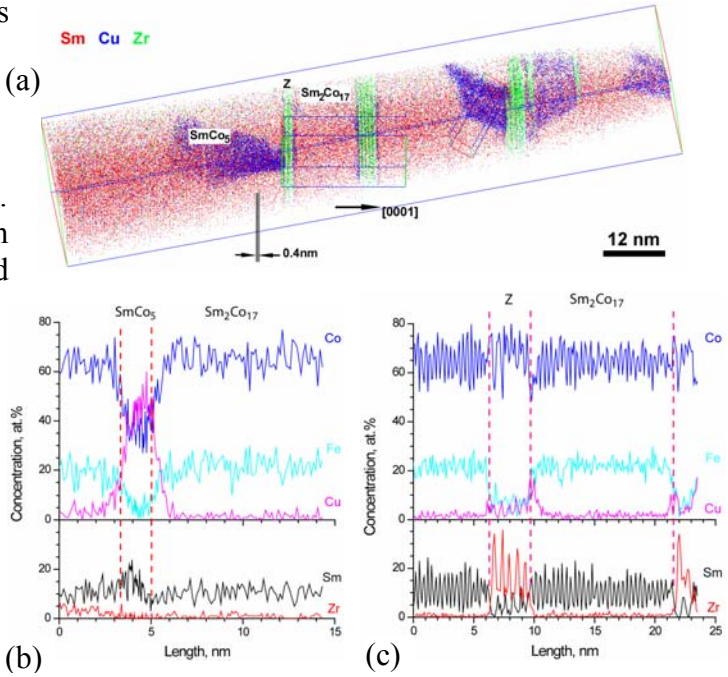

Fig. 4. (a) 3D atom maps of Sm, Cu and Zr, and composition profiles across (b) the $SmCo_5$ phase (box size = 6×7×14 nm^3) and (c) the Z phase (box size = 6×14×24 nm^3), as shown in (a), for the sample ages at 840°C.

Table 1. Phase compositions following 720 and 840°C ageing.

		Composition, at.%				
Sample	**Phase**	***Sm***	***Co***	***Fe***	***Cu***	***Zr***
720°C	$SmCo_5$	12.5 ± 0.4	38.9 ± 0.5	5.0 ± 0.4	42.9 ± 0.5	0.8 ± 0.2
	Sm_2Co_{17}	10.6 ± 0.4	64.5 ± 0.5	21.0 ± 0.5	2.0 ± 0.4	1.9 ± 0.4
840°C	$SmCo_5$	13.4 ± 0.4	37.4 ± 0.5	4.3 ± 0.2	44.5 ± 0.5	0.4 ± 0.2
	Sm_2Co_{17}	10.8 ± 0.4	64.7 ± 0.5	22.0 ± 0.4	1.7 ± 0.2	0.8 ± 0.2
	Z-phase	5.2 ± 0.2	70.6 ± 0.5	7.4 ± 0.2	3.8 ± 0.2	13.0 ± 0.2

higher activation energy for its formation. This result does not support the model proposed by Ray for the metallurgical behaviour of these alloys [7,8], which proposes that at the isothermal ageing temperatures, the strong tendency for the formation of the Sm_2Co_{17} structure is initiated by the precipitation of the Z-phase, resulting in a matrix phase of 2:17 stoichiometry, and the Cu-rich $SmCo_5$ phase was subsequently precipitated due to the supersaturated Cu in the matrix phase. The transformation sequence proposed by Maury *et al*. [9], in which rapid nucleation and growth of the Sm_2Co_{17} phase occurs during the isothermal ageing and the $SmCo_5$ phase forms in the surrounding matrix, while the Z-phase is formed during a less rapid series of transformations during isothermal ageing at the cost of the $SmCo_5$ phase, is consistent with our results.

Comparing the changes in the microstructures and the magnetic properties, the increases in H_c, $(BH)_{max}$ and M_r/M_s with ageing is attributed to the formation of the cellular structure consisting of the Sm_2Co_{17} and $SmCo_5$ phases. Similar to the conventional, SmCo-based, permanent magnets for which Cu was enriched in the $SmCo_5$ phase to ~20 at.% [4], this melt-spun alloy showed even higher Cu contents, ~44 at.%, in the $SmCo_5$ phase, but the H_c was much lower, which may suggest that the coercivity is controlled by other effects, rather than by the Cu concentration gradient. As both XRD and TEM showed the presence of a CoFeZr-rich phase in the aged samples, and the grain size of this phase increased with increasing ageing temperature, the degradation in H_c, $(BH)_{max}$ and M_r/M_s is controlled by the increase in the volume fraction of this soft magnetic phase, and this also accounts for the increase in σ_s.

Acknowledgments

An Australian Research Council (Discovery) Grant is acknowledged.

References

[1] K.J. Strnat in *Ferromagnetic Materials*, eds. E.P. Wolfarth and K.H.J. Buschow, (Elsevier, Amsterdam, 1988) Vol 4, p 131.
[2] J.F. Liu, Y. Ding, Y. Zhang, D. Dimitar, F. Zhang and G.C. Hadjipanayis, *J. Appl. Phys.* **85**, 5660 (1999).
[3] W. Tang, Y. Zhang, J.F. Liu, C.H. Chen and G.C. Hadjipanayis, *Proceedings 16th International Workshop on Rare-Earth Magnets and Their Applications*, eds. H. Kaneko, M. Homma and M. Okada (Japan Inst. Metals, 2000) p 179.
[4] X.Y. Xiong, T. Ohkuba, T. Koyama, K. Ohashi, Y. Tawara and K. Hono, *Acta Mater.* **52**, 737 (2004).
[5] A. Cerezo, T.J. Godfrey, S.J. Sijbrandij, G.D.W. Smith and P.J. Warren, *Rev. Sci. Instr.* **69**, 49 (1998).
[6] X.Y. Xiong and T.R. Finlayson, *Ultramicroscopy*, **107**, 781 (207).
[7] A.E. Ray, *J. Appl. Phys.* **67**, 4972 (1990).
[8] A.E. Ray and S. Liu, *J. Mater, Eng. & Perform.* **1**, 183 (1992).
[9] C. Maury, L. Tabenberg and C.H. Allibert, *phys. stat. sol. (a)*, **140**, 57 (1993).